Rectification Properties and pH-Dependent Selectivity of Meningococcal Class 1 Porin

Javier Cervera,* Alexander G. Komarov,† and Vicente M. Aguilella*
*Departamento de Física, Universitat Jaume I, 12080 Castellón, Spain; and †Vollum Institute, Oregon Health and Science University, Portland, Oregon

ABSTRACT We studied the current rectification properties and selectivity of class 1 porin (PorA) from *Neisseria meningitidis* (strain H44/76 Δ3Δ4) reconstituted in planar lipid membranes varying salt concentrations and pH. PorA channel shows voltage gating with a characteristic time remarkably longer than other porins. Its current-voltage asymmetry, evaluated as the current rectification ratio, changes nonmonotonically with salt concentration. Interestingly, it reaches its maximum value at physiological concentration. Porin selectivity, quantified by reversal potential measurements, is also significantly asymmetric. Depending on the direction of the salt gradient, the channel becomes more or less selective (10:1 vs. 5:1 Na^+/Cl^-). Besides, the reversal potential measurements suggest that porin inserts directionally following the concentration gradient. Measurements over a wide range of pH show that although PorA is strongly cation selective at pH >6, its selectivity gradually changes to anionic in an acidic medium (pH < 4). We show that a continuum electrodiffusion model quantitatively accounts for conductance and reversal potential measurements at positive and negative applied voltages.

INTRODUCTION

Porins form large water-filled channels in the outer membrane of Gram-negative bacteria. They are designed to allow the exchange of small hydrophilic molecules, thereby regulating the influx of nutrients and the efflux of waste products (1). Some of these protein channels specialize in facilitating the transport of specific solutes (2), whereas others are general diffusion porins. General porins allow the passage of small compounds at a high rate, but some—like OmpF, OmpC, and class 1 porin (PorA)—also display some cationic selectivity, and others—like Omp32, Omp34, PhoE, and PorB—also display some anionic selectivity (3–7).

The bacterium *Neisseria meningitidis* contains four classes of major outer membrane proteins (OMP): class 1, also named PorA; class 2/3, named PorB; and classes 4 and 5 (8). PorAs are homologous within any strain but exhibit antigenic heterogeneity between them (9–14). This is reflected in their similar but quantitatively different biophysical properties such as selectivity, conductance, and voltage gating. The interest in a detailed biophysical characterization of Neisserial porins comes from their role as pathogenesis effectors (15), their effect on the immune system, and their interaction with the mitochondria of target cells, where they appear to modulate apoptosis (16). In particular, the class 1 major OMP of *N. meningitidis* is a promising candidate for a meningococcal vaccine (8,17,18). Therefore a better understanding of PorA structure and an explanation of its unique properties will undoubtedly lead to the improvement of vaccines/antibodies against bacterial meningitis.

To date no crystallographic structure of any complete PorA protein has been resolved. However, information about its structure has been inferred from the comparison of amino acid sequences of different strains, as well as from homology models based on known structures of *Escherichia coli* porins (9,10,14). Based on a folding pattern proposed by Van der Ley and co-workers (10), Song et al. (5) suggested a tentative tertiary structure for the PorA channel (strain H44/76 Δ3Δ4) consisting of a neutral part and a selectivity filter.

The goal of this study is to characterize the rectification and selectivity properties of the channel formed by the PorA protein (*N. meningitidis*) reconstituted in planar lipid membranes. By combining conductance and reversal potential measurements with continuum electrodiffusion calculations, we indirectly obtain information about the porin tertiary structure and the charged amino acid residues responsible for the channel selectivity. Upon the reversal change of the salt concentration gradient, we find that the channel asymmetric structure is reflected in the asymmetry of the ion selectivity and that channel insertion depends on the direction of the salt gradient, a novel feature whose origin and functional implications are unclear. We also rationalize the change in current rectification with salt concentration in terms of a pore model (5) where transport properties are determined not by the charged selectivity filter but by the overall protein structure and charge distribution (19–21).

MATERIALS AND METHODS

Channel reconstitution and transport measurements

Planar membranes were formed from monolayers made from a solution containing 1% diphytanoylphosphatidylcholine (Avanti Polar Lipids, Alabaster, AL) in pentane. The two monolayers form a bilayer membrane across a 70–90-μm diameter aperture in a 15-μm thick Teflon partition that separates two chambers (modified Montal and Mueller technique (22)). The orifices

Submitted July 9, 2007, and accepted for publication September 25, 2007.

Address reprint requests to Vicente M. Aguilella, E-mail: aguilell@fca.uji.es.

Editor: Robert Hsiu-Ping Chow.

0006-3495/08/02/1194/09 $2.00

doi: 10.1529/biophysj.107.116186

were pretreated with a 1% solution of hexadecane in pentane. The total capacitance depended on the actual position of the orifice in the partition but was always ~50–100 pF. NaCl solutions were used either unbuffered or, for those with a controlled pH value, buffered with 5 mM HEPES. The meningococcal PorA protein (strain H44/76 Δ3Δ4) was kindly provided by Dr. Milan Blake. Channel insertion was achieved by adding a 0.1–0.2 μl aliquot in a 1% Triton X-100 solution of purified PorA to the 2.0 ml aqueous phase in one of the compartments while stirring. The membrane potential was maintained using Ag/AgCl electrodes with 2 M KCl, 15% agarose bridges assembled within standard 200 ml pipette tips (23). Potential is defined as positive when it is greater at the side of protein addition (*cis*). An Axopatch 200B amplifier (Molecular Devices, Sunnyvale, CA) in the voltage-clamp mode was used for measuring the current and applying potential. Data were filtered using the internal four-pole low-pass Bessel filter of the amplifier at 10 kHz and saved directly into the computer memory. The membrane chamber and the head stage were isolated from external noise sources with a double metal screen (Amuneal Manufacturing, Philadelphia, PA). All measurements were made at room temperature (25°C ± 1°C).

Single-channel insertions were observed as a stepwise increase of the membrane conductance. The properties of PorA such as voltage gating and high cation selectivity (see Results and Discussion section) allowed us to separate channel insertions from nonselective and nonspecific membrane leaks. To estimate single-channel conductance, we selected an interval when the three monomers were open and averaged the measured current. Reversal potential for the single channel was also measured. We measured the applied potential required to zero the current generated by a salt concentration gradient across the membrane. This value was then corrected for the liquid junction potentials at the interfaces between the solutions and the salt bridges of the electrodes. At least three independent experiments were performed for each experimental point on the graphs.

Perfusion protocol

Reversal measurements suggested directional insertion of the channel, with its orientation being set by the salt concentration gradient (see Channel selectivity and orientation section). To test this possibility, we devised a special protocol of channel insertion to measure the reversal potential with inverted concentration gradient. It was based on the assumption that channels do not change their orientation after insertion into a membrane. PorA was initially inserted in the presence of a fourfold NaCl gradient 0.10 M *cis*/0.05 M *trans*. Then, 0.5 ml of the *trans* solution was exchanged by a concentrated NaCl solution to reverse the gradient up to the desired value. Stirring was then applied to mix the *trans* solution.

RESULTS AND DISCUSSION

Current rectification

A typical single-channel recording for 1 M NaCl and −150 mV of applied voltage is shown in Fig. 1 *a*. The porin displays voltage gating for applied voltages around ±80 mV and higher. Single porin closure is observed in three discrete steps, each one being one-third of the total current. This confirms the trimeric nature of the porin which had been predicted by its biochemical characterization (5). Fig. 1 *b* shows two recordings made at high sampling frequency (20 kHz) for a single channel at +150 mV (*top trace*) and −150 mV (*bottom trace*). We found that current noise amplitude was higher for positive than for negative applied voltages. This property has also been observed in OmpF porin (24), but its origin remains unclear.

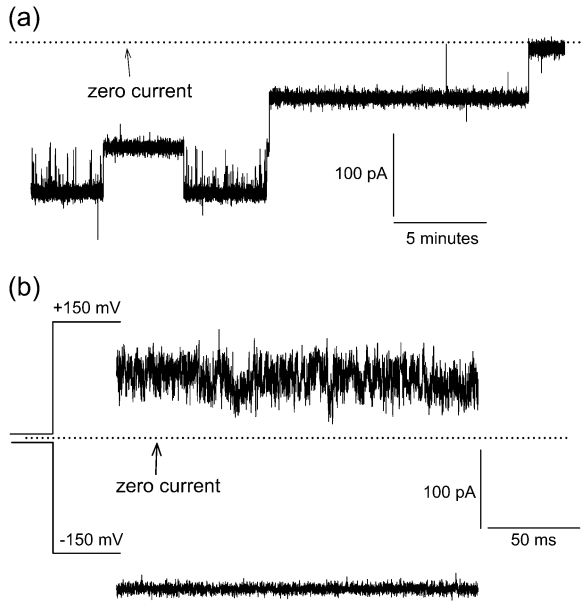

FIGURE 1 (*a*) Recording of single-channel ion current in 1 M NaCl at pH 7 that illustrates the triggering of voltage gating at −150 mV. Single porin closures are observed in three discrete steps, each one being one-third of the single-channel conductance. The closure process is far slower than reported for other porins. Characteristic time is in the range of minutes. (*b*) Comparison between the current for applied voltage of +150 mV (*top trace*) and −150 mV (*bottom trace*).

The first observations showed that PorAs are slightly voltage dependent at physiological potentials (8). However, PorA P1.6 and P1.7,16 were reported to exhibit voltage gating at potentials higher than ±80 mV (25). Earlier studies on the PorA strain used here (H44/76 Δ3Δ4) have not detected voltage gating (5). This can probably be explained by the closure time of the porin, which is in the range of minutes. Closure time is much larger than has been reported for other porins (20,26).

Raising the transmembrane potential over 80 mV induces voltage gating, and the number of monomer closures can be estimated. That allows us to determine the single-channel conductance. Fig. 2 shows single-channel current-voltage curves for different NaCl concentrations at pH 7. The porin displays current rectification, and therefore its conductance depends on both the magnitude and the polarity of the applied voltage. In 1 M NaCl the conductance is 1.0 nS (at +20 mV), which is similar to the 0.73 nS reported for PorA P1.6 (25).

Channel selectivity and orientation

We studied PorA cationic selectivity by measuring reversal potential. The first series of measurements was performed at pH 7 for a fixed *trans* concentration of 0.1 M NaCl and different salt concentrations on the *cis* side (Fig. 3). The reversal potential of an ideal cation-selective channel (from the Nernst equation) is also shown (*dashed line*) for comparison.

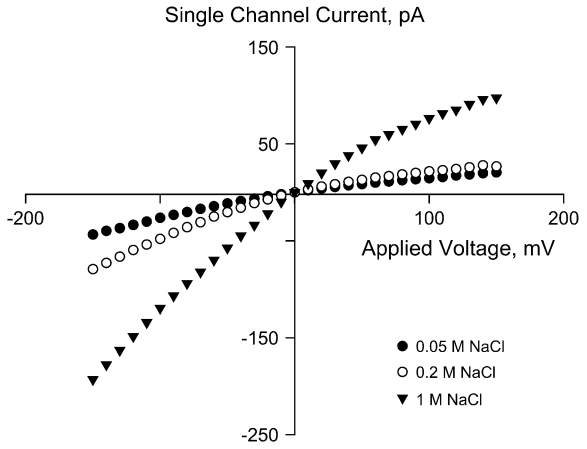

FIGURE 2 Current-voltage dependence for a single PorA channel for different NaCl concentrations at pH 7. The current-voltage curve is strongly asymmetric even for 1 M NaCl.

The porin is highly cation selective for *cis* concentrations below 1 M. However, for higher concentrations its selectivity gradually increases less than the ideal cation selectivity.

The observed selectivity lies along the generalized consensus about the cation selectivity of PorA porins (5,8,25). However, quantitatively, selectivity varies greatly with the specific strain. PorA P1.6 (strain M990) and P1.7,16 (strain H44/76) show moderate cation selectivity (5.6:1 K^+ over Cl^- for P1.6 and 6.4:1 for P1.7,16) (8,25), whereas Song and co-workers estimated a selectivity of up to 23.5:1 K^+ over Cl^-, at low salt concentrations, for the same PorA (strain H44/76 Δ3Δ4) used in this study (5). Still, any comparison between reported selectivity measurements should be done with care because of the disparity in the experimental conditions, particularly those of solution pH and concentration gradient.

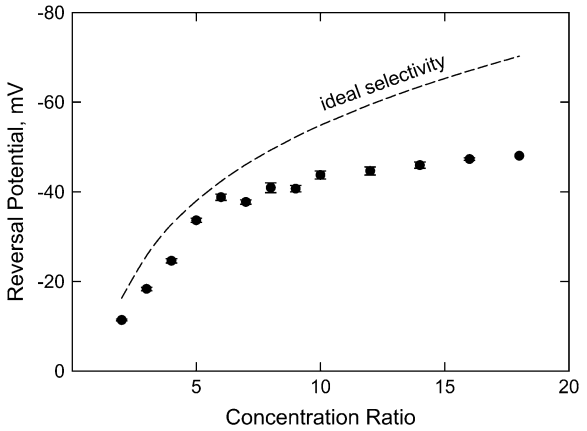

FIGURE 3 Reversal potential in NaCl at pH 7 as a function of the concentration ratio. The *trans* side concentration is kept constant at 0.1 M, whereas the *cis* side concentration is varied. For comparison purposes, the reversal potential of an ideal cation-selective channel is also displayed (*dashed line*).

We also measured the reversal potential for inverted concentration ratios, i.e., we kept a fixed *cis* concentration of 0.1 M and increased *trans* concentration. The results obtained did not differ from those reported in Fig. 3 except for the reversed sign of the potential (data not shown). This is what could be expected for a symmetric channel, where selectivity does not depend on the direction of the salt gradient. However, in an asymmetric channel, the reversal potential should not only reverse its sign but also change in magnitude upon inversion of the concentration gradient (20). Thus, obtaining the same absolute values implies either that the porin selectivity does not depend on the direction of the salt concentration gradient or that the channel insertion follows the concentration gradient. In this second case, the porin would have the same orientation with respect to the concentration gradient as in Fig. 3. To sort it out, a special perfusion protocol was devised (see Materials and Methods) so that in both sets of measurements (i.e., constant *trans* concentration and constant *cis* concentration) the initial concentration was higher on the *cis* side than on the *trans* side. We found a reproducible reversal potential asymmetry, which shows that the channel is not equally selective upon inversion of the salt concentration gradient (Fig. 4). This asymmetry is greater than that reported for the OmpF channel (20). Unfortunately, for high concentrations on the *trans* side (*open squares*), the channel became unstable and no reproducible results could be obtained for a concentration ratio of 10 or higher.

The results for the reversal potential at inverted concentration ratios support the hypothesis that the channel inserts directionally following the concentration gradient. This conclusion is in agreement with the directional insertion of the porin in symmetric solutions, which was observed by Song and co-workers using an antibody approach (5). According to their interpretation, porin inserts with the (in vivo) surface-exposed loops facing the *trans* side. In this region they predicted the existence of a negatively charged, narrow part of the channel forming a filter. In our selectivity measurements, the channel seems to insert with the negatively charged filter facing the low concentration side (the *trans* side in the first series of experiments, corresponding to the *solid circles* in Fig. 3). Once the salt gradient is reversed, the channel becomes unstable when the negatively charged filter faces a *trans* side solution, which is much more concentrated than a *cis* side solution. Currently we do not have a good explanation for this phenomenon.

Residue ionization

The small difference between the reversal potential measured in neutral (pH 7) versus unbuffered solutions (compare the data in Fig. 3 to the corresponding set in Fig. 4) suggests that channel selectivity is pH dependent. We systematically measured the reversal potential as a function of the pH for a constant NaCl concentration ratio of 1 M *cis*/0.1 M *trans* (Fig. 5).

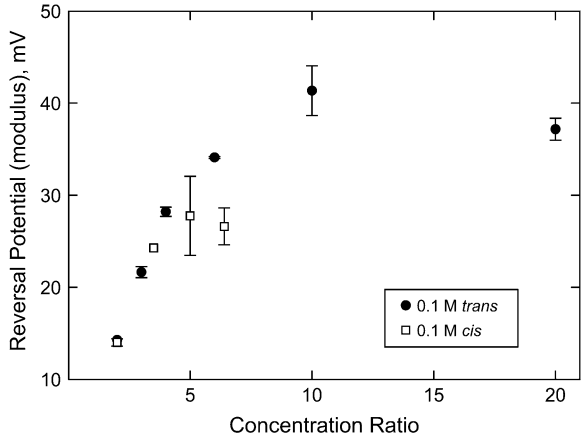

FIGURE 4 Reversal potential in NaCl for different salt gradients. The lower concentration is kept constant at 0.1 M in all experiments. Salt concentration in the other solution is varied to obtain the desired concentration ratio. Solutions are unbuffered. An asymmetry parallel to that of current-voltage curves is observed when the concentration ratio is reversed. The measurements with 0.1 M on the *cis* side (*squares*) were done using a perfusion method (see main text).

Although PorA is strongly cation selective at neutral pH (negative reversal potential), it becomes anion selective for very low pH (pH $<$ 4). The shape of the channel titration curve is consistent with the neutralization of several acidic residues with the same or very close effective pK_a. The dot curve in Fig. 5 was calculated according to the following expression (27):

$$E(\mathrm{pH}) = E_{\min} + \frac{E_{\max} - E_{\min}}{1 + 10^{\mathrm{pH}-\mathrm{pKa}}},$$

where E denotes the reversal potential. The best-fit parameters are $E_{\max} = 38.0$ mV, $E_{\min} = -43.4$ mV, and $pK_a = 4.3$.

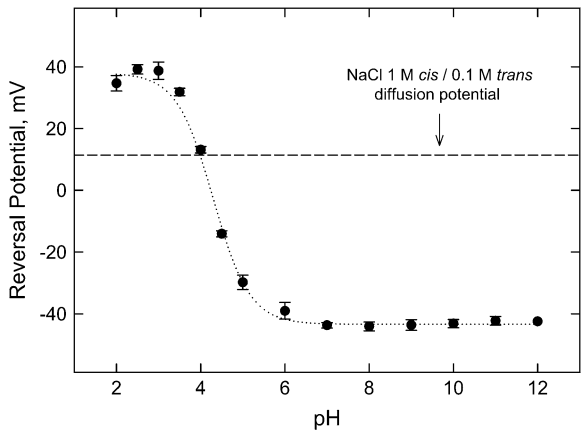

FIGURE 5 Reversal potential as a function of pH in 10-fold NaCl concentration gradient (1 M *cis*/0.1 M *trans*). At high pH the porin is cation selective but gradually turns into anion selective at low pH, when the acidic residues are fully protonated. The curve is similar in shape to a titration curve of an acidic residue with $pK_a \sim 4.3$ (*dotted line*).

Data suggest a porin ''isoelectric point'' of pH ~4, where reversal potential (12.4 ± 1.0 mV) is close to the bulk diffusion potential of NaCl for a 10-fold concentration gradient (11.4 mV). This diffusion potential would be the reversal potential measured in a hypothetical neutral, inert pore (28). The above pK_a value of 4.3 is consistent with a selectivity filter with several aspartic (pK_a 4) and glutamic (pK_a 4.4) amino acids, as hypothesized by Song et al. (5) on the basis of the folding pattern of PorA proposed by van der Ley et al. (10). According to these authors two clusters of negative charges at one end of β-strands 2–5 and in loop 5 (Fig. 9 in McGuinness et al. (5)) would account for the channel cationic selectivity. The question remains about which basic residues are responsible for the channel anionic selectivity at low pH. The shape of the titration curve at the high pH end reveals no apparent change in the channel net charge over a wide range of basic pH. This might indicate that any basic residue contributing to the anionic selectivity should have an effective $pK_a > 13$. The pK_as of arginines, lysines, and tyrosines in free solution are below 13, but electrostatic calculations in other porins show that a low dielectric environment induces a positive pK_a shift in basic residues (3,20). Therefore, we cannot exclude the possibility that several positively charged residues lie near the channel constriction.

Continuum electrodiffusion model

Both the current rectification (Fig. 2) and the asymmetry in the reversal potential for a reversed concentration gradient (Fig. 4) suggest that the porin has an asymmetric structure and charge distribution. In addition, the strong cation selectivity displayed by the porin at pH 7 (Fig. 5) implies that the channel should be highly negatively charged at this pH. This is consistent with the channel three-dimensional (3D) structure proposed by Song et al. (5). The existence of a negatively charged filter explains the porin cationic selectivity; its position on one side of the channel would be responsible for the asymmetries found in the conductance and reversal potential.

It is known that many bacterial porins with low selectivity, either cationic (20) or anionic (29,30), demonstrate permeation properties regulated mainly by long-range electrostatic interactions. We show here that ion transport across strongly selective porins like PorA can also be accurately described by means of a continuum electrodiffusion approach where only electrostatic interactions between the channel charged residues and the permeant ions are considered. Particularly, some features of the current-voltage curve and the change of selectivity with salt concentration can be quantitatively explained. We used a model based on a two-dimensional (2D) numerical solution of Poisson-Nernst-Planck (PNP) equations (see Appendix) on a domain that includes the pore itself and the surrounding solutions (so that access resistance is accounted for). Despite its limitations, the PNP continuum approach (31) has proved reliable in wide pores (radius ~1 nm),

whose transport properties are mainly determined by long-range electrostatic interactions (20,21,32–36). Details about the equations, the boundary conditions, and the pore geometry used are given in the Appendix. The aim of the following model calculations is to quantitatively assess the agreement between the assumed channel 3D structure and our measurements, with one additional assumption: ion transport is regulated by electrostatic interactions between the charges of ionizable residues and permeating ions.

If we look in detail into the channel conductance asymmetry, estimated by the current rectification ratio $I(-V)/I(+V)$, we find that it is concentration dependent (Fig. 6). It is higher at intermediate salt concentrations (0.2 M) than at high (1.0 M) and low (0.05 M) NaCl concentrations. Interestingly, the maximum rectification ratio is observed at physiological concentrations. This nonmonotonic change of the current ratio with NaCl concentration can be rationalized by computing the spatial profiles of Na^+ and Cl^- concentration across the channel and the surrounding solutions for both voltage polarities.

According to the assumed 3D channel structure, the pore is divided into two regions: the filter and the neutral part. Due to the electroneutrality condition, the net space charge (i.e., the difference between the number of Na^+ and Cl^- ions) must cancel out the fixed charges in the filter region. However, the absolute value of the Na^+ and Cl^- concentrations is not fixed but depends basically on the availability of Na^+ ions to enter the filter (only the difference between positive and negative ions must remain constant). If Na^+ concentration is low, then the fixed charges are poorly screened and Cl^- ions are excluded from the filter region due to the electrostatic repulsion. As the number of Na^+ ions increases, the fixed charges are better screened, and more and more Cl^- ions are allowed to enter the filter region. The overall effect is that there is a smaller ionic concentration inside the porin when the access of Na^+ ions to the filter is restricted. The access of Na^+ ions to the filter is limited by the neutral part of the porin. In symmetric solutions, the porin inserts with the filter facing the *trans* side (5). In our case, this implies that at negative voltages, Na^+ ions enter the channel through the filter region and exit through the neutral region, and at positive voltages Na^+ ions enter through the neutral region and exit through the filter. Therefore, fewer Na^+ ions reach the filter for positive than for negative applied voltages. The calculated ion concentration profiles plotted in Fig. 7, together with an outline of the channel orientation, illustrate the difference in counterion accumulation and coion exclusion under positive and negative voltages. Model calculations predict a smaller ionic concentration inside the porin for positive than for negative potentials. This would explain the different conductance observed in each case.

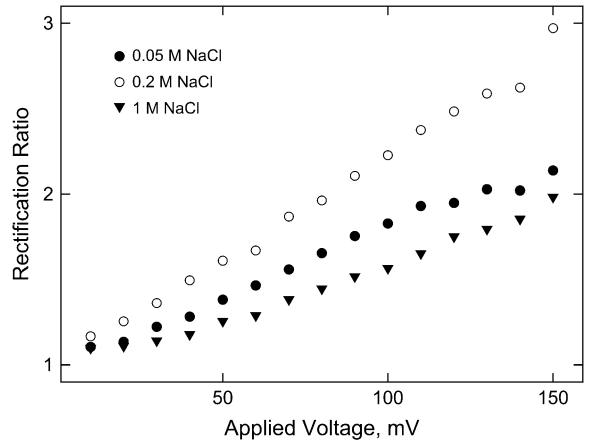

FIGURE 6 Absolute value of the current ratio $I(-V)/I(+V)$ for the current-voltage curves shown in Fig. 2. A nonmonotonic change of the current ratio with maximum values at intermediate concentrations is seen.

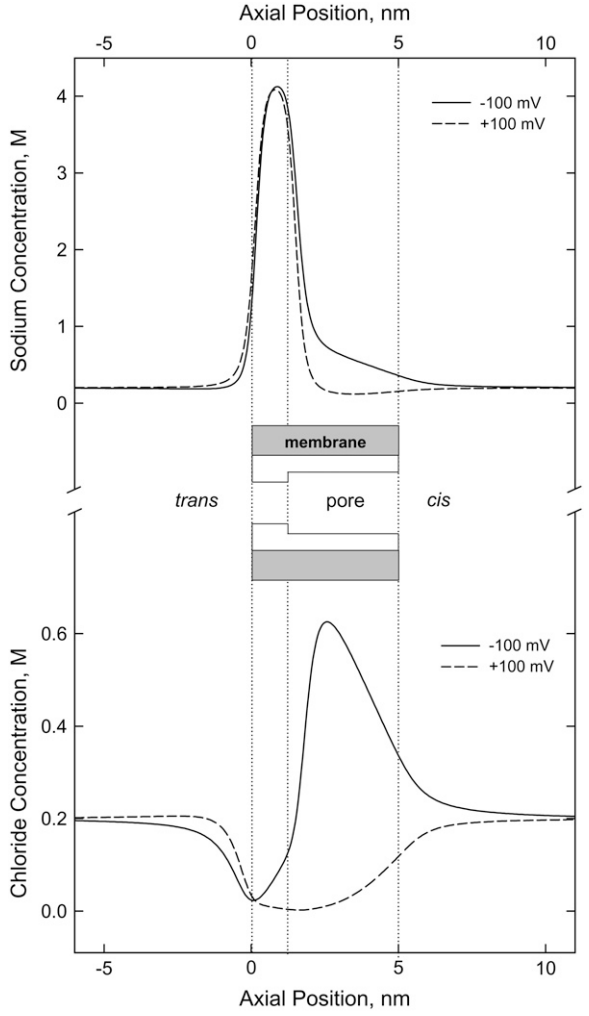

FIGURE 7 Model calculations of ion concentration spatial profiles across the pore and the surrounding solutions (calculated along the pore longitudinal axis). An outline of the channel structure and its orientation in the lipid membrane is also shown. Solid and dashed lines denote the concentration for negative and positive applied potentials on the *cis* side, respectively.

Two limiting cases naturally arise from this description of the porin asymmetric conductance. At very low salt concentrations, the availability of Na^+ ions to the filter is low regardless of the direction of the current. In this limit, there are only Na^+ ions in the pore since Cl^- ions are almost totally excluded. The Na^+ concentration is then fixed by the condition of electroneutrality regardless of the sign of the applied voltage, which eliminates the asymmetry of the current-voltage curve. By contrast, in the high salt concentration limit, the availability of Na^+ ions to the filter is high regardless of the applied potential. The fixed charges are then strongly screened, and their effect on the ionic transport is highly reduced. This also leads to a low current-voltage asymmetry. In between these two limits, the current rectification has a nonmonotonic behavior, attaining a maximum value at an intermediate salt concentration. This would explain why the rectification ratio is higher at 0.2 M than at 1 M or 0.05 M.

Fig. 8 shows the calculated current voltage curves. The ionic diffusion coefficients used in calculations are one-fifth of the infinite solution values for both ions (this correction factor is the only fitting parameter used). The model correctly accounts for the asymmetric conductance but overestimates the rectification ratio at high salt concentration. In addition, the model predicts the observed nonmonotonic dependence of the current rectification with salt concentration, although the maximum is shifted toward higher concentrations: According to theory, channel rectification is at its maximum at 0.8 M, whereas experiments suggest that the channel rectification maximum is reached at concentrations around 0.2 M. The discrepancies between theory and experiment can be ascribed to model limitations as well as to the inferred structure of the porin.

We attributed the asymmetry of the current-voltage curve to the different ionic concentrations in the porin for positive and negative applied potentials. Since the model neglects the finite size of the ions, it overestimates the difference between the ionic concentrations for positive and negative applied potentials and, consequently, the current rectification ratio.

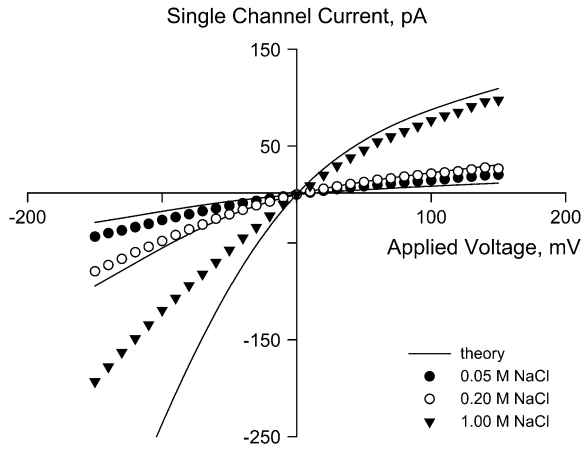

FIGURE 8 Comparison of the theoretical prediction of the current-voltage curves (*solid lines*) with the measured values (*points*). The theoretical model is based on PNP-2D equations applied to the inferred structure of the porin (5). The diffusion coefficients are used as fitting parameters. Their best fit is one-fifth of the infinite dilution value.

Notwithstanding the limitations of the model, the uncertainty in the 3D structure of the porin partially explains the discrepancy between the model predictions and the measured current-voltage curves. For example, if the filter spanned longer in the porin, its charges would be more evenly distributed. This would cause a decrease in the asymmetry of the conductance as well as a shift of the maximum of the current rectification toward a smaller concentration.

The above explanation for current-voltage rectification is linked to the asymmetry observed in the porin selectivity. The difference between Na^+ and Cl^- ion concentration inside the channel is bound to cancel out the fixed charges of the filter. Therefore, the high ionic concentration associated with the negative applied potential implies low cationic selectivity of the porin. By analogy, the small ionic concentration for positive applied potentials yields a high ionic selectivity. Although the conditions are not the same, the dependence of the porin selectivity on the ionic flux direction can be observed in Fig. 4. In measurements with 0.1 M NaCl on the *trans* side, the ions enter the pore through the neutral region, whereas in experiments with 0.1 M on the *cis* side, they enter through the filter region. In the latter case, selectivity is weaker due to the increased screening that results from the higher ionic concentration inside the pore.

The reversal potential measurements reported above (Figs. 3 and 4) show that the selectivity of the porin is asymmetric and highly cationic. By analogy with other wide channels (20,21) one can guess that the channel 3D structure and the space distribution of charged residues are likely to determine those selectivity properties. Although we know neither the details of channel geometry nor the charge distribution and merely make some assumptions (5), we calculated the reversal potential for several concentration gradients on the basis of the model described above (see details in the Appendix). As shown in Fig. 9, theory calculations and data from experiments compare reasonably well. This agreement is remarkable since no attempt has been made to fit the experimental results: the proposed pore structure (5) has been used and the modified ionic diffusion coefficients have no effect in the calculation, since the ratio D_+/D_- remains unchanged. The model correctly predicts the variation of the reversal potential with the concentration ratio. The initial rise in reversal potential is associated with the higher ion flux brought on by the increase of the concentration ratio. The decrease of the slope of the curve for high concentration ratios is linked to the weakening of the porin selectivity. A high concentration ratio implies a high concentration value on the *cis* side, which screens the fixed charges more effectively.

The asymmetry of the reversal potential with the direction of the concentration gradient is also well reproduced by the model. Note that in this case the measurements were made in

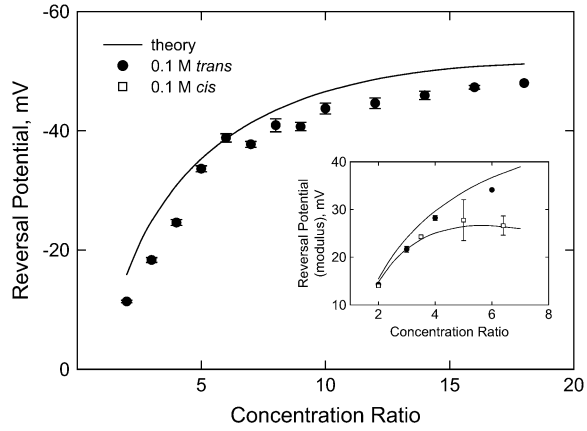

FIGURE 9 Main panel: comparison of reversal potential measurements (pH 7) and theory calculations over the whole range of concentration ratios explored. The inset shows both calculations and measurements for the two directions of the concentration gradient (these measurements were made in unbuffered solutions).

unbuffered solutions (pH ~5). As can be seen in the titration curve (Fig. 5), at pH 5 the reversal potential (and hence channel fixed charge) is slightly lower in modulus than at pH 7. Therefore, in the calculations shown in the inset we used a proportionally smaller surface density.

It is common to report channel selectivity in terms of the permeability ratio derived from the well-known Goldman-Hodgkin-Katz equation (37,38). It is interesting to note that the cation/anion permeability ratio (P_{Na}/P_{Cl}) changes twofold when the concentration gradient is reversed: from 5:1 for 0.1 M NaCl in the *cis* side to 10:1 for 0.1 M NaCl in the *trans* side. Therefore, the porin selectivity seems higher when the selectivity filter is facing the low concentration solution.

Experiments and model calculations show that PorA selectivity seems more sensitive than current-voltage curves to the asymmetry of the channel 3D structure. This has also been observed in OmpF, where the asymmetry in the structure is revealed not in the current rectification but in the dependence of the reversal potential with the direction of the concentration gradient (20).

CONCLUSIONS

We studied the rectification and selectivity properties of the PorA channel by means of conductance and reversal potential measurements in NaCl solutions under several conditions of salt concentration and solution pH. Our main conclusions can be summarized as follows:

1. The channel shows voltage gating with characteristic time (minutes) much longer than other porins. Stepwise monomer closures allowed reliable determination of single-channel conductance.
2. PorA exhibits a strong current rectification that varies nonmonotonically with salt concentration. The channel conductance changes up to threefold upon reversing polarity. The current noise amplitude observed for positive applied potential on the side of protein addition is considerably greater than for the reversed bias.
3. Measured channel selectivity is asymmetric. The reversal potential depends on the direction of the salt gradient.
4. The results obtained for the reversal potential suggest that the porin inserts directionally following the concentration gradient.
5. PorA selectivity is pH dependent. The strong cationic selectivity of the porin switches to anionic in acidic solutions. The titration curve is consistent with the existence of one or more types of ionizable residues with pK_a ~4.3.
6. The previously proposed channel tertiary structure based on a neutral part of the pore and a highly charged selectivity filter near one end of the pore is fully supported by our results.
7. A macroscopic electrodiffusion model based on electrostatic interactions between the charges of ionizable residues and permeating ions accounts semiquantitatively for current rectification, reversal potential change with salt concentration, and reversal potential asymmetry.

APPENDIX

Our electrodiffusion model is based on the PNP formalism and on the PorA structure proposed by Song and coauthors (5). The flux density of ionic species i is described by the Nernst-Planck equation

$$\mathbf{j}_i = -\frac{D_i c_i}{RT}\nabla(RT\ln a_i + z_i F\phi), \quad i = \pm, \tag{A1}$$

where D_i, c_i, a_i, and z_i are the diffusion coefficient, concentration, activity, and charge number of species i, respectively, ϕ is the electric potential, R is the gas constant, T is the temperature (assumed constant), and F is the Faraday constant. We consider the system in the steady state, so that the continuity equations read

$$\nabla \cdot \mathbf{j}_i = 0, \quad i = \pm. \tag{A2}$$

It is assumed that the behavior of the system is controlled by long-range electrostatic interactions. In the model, this is described by the Poisson equation

$$\nabla^2\phi = -\frac{F}{\varepsilon}(c_+ - c_-), \tag{A3}$$

where ε is the dielectric permittivity of the solution, assumed to be constant for the whole solution. We further assume that the aqueous boundaries outside the porin are perfectly stirred and that there is no convection.

The pore geometry and charged residue distribution set the calculation domain and boundary conditions for the system, which are shown in Fig. 10. The pore is assumed to have cylindrical symmetry. In the calculation we take into account the area of the porin inaccessible to the ions due to their size (36). This is done by reducing the pore size by the hydrated Na^+ radius, since all experiments were done in NaCl and Na^+ ions are more likely to be close to the porin walls lined with negative residues.

The acidic residues are modeled as a (negative) surface charge density σ smeared on the filter walls. The electrolyte concentration and electric potential in *cis* and *trans* solutions, far from the porin entrances, are denoted by c^{cis}, c^{trans} and ϕ^{cis}, ϕ^{trans}. At the pore walls the ion flux directed toward them must vanish. Then

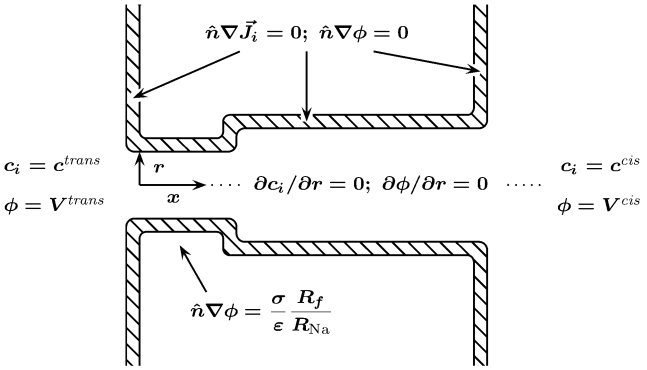

FIGURE 10 Schematic view of the domain used in the theoretical calculation along with the boundary conditions. The hatched area represents the region from which the ions are excluded due to their hydrated radii. The domain extends far away from the porin (at least 10 times the filter radius), where the bulk values of the concentration and electric potential are set as boundary conditions.

$$\mathbf{n} \cdot \mathbf{j}_i = 0 \,(\text{porin walls}), \tag{A4a}$$

where **n** is the normal vector of the surface porin wall. In the lipid region we assume a dielectric permittivity low enough to neglect the electric field there. The boundary conditions for the electric potential are then

$$\mathbf{n} \cdot \nabla\phi = 0 \,(\text{at neutral pore walls}) \tag{A4b}$$

except for the filter walls where Gauss law implies that

$$\mathbf{n} \cdot \nabla\phi = \frac{\sigma}{\varepsilon}\left(\frac{R_f}{R_f - R_{Na}}\right) (\text{at the filter walls}), \tag{A4c}$$

where R_f is the radius of the selectivity filter and R_{Na} is the hydrated Na^+ radius. Note that Gauss law is modified by a factor $R_f/(R_f - R_{Na})$ to preserve electroneutrality in the porin cross section (39). Finally, the cylindrical symmetry yields two more boundary conditions at the channel symmetry axis ($r = 0$):

$$\frac{\partial c_i}{\partial r} = 0 \tag{A4d}$$

$$\frac{\partial \phi}{\partial r} = 0. \tag{A4e}$$

Equations A1–A3, subject to the boundary conditions (Eq. A4), form the system of transport equations. The electric current across the pore is then calculated as

$$I = F(J_+ - J_-), \tag{A5}$$

where J_+ and J_- are the fluxes of Na^+ and Cl^- ions

$$J_i = 2\pi \int_0^{R(x)} j_{i,x} r \mathrm{d}r, \quad i = \pm \tag{A6}$$

and $j_{i,x}$ is the axial component of the corresponding flux density. Current-voltage curves are obtained by calculating the current for different applied voltages $V = \phi^{cis} - \phi^{trans}$. Reversal potential values are calculated by setting a concentration difference $c^{cis} - c^{trans}$ and obtaining the applied voltage that gives zero current using an iterative method. In the calculations, the temperature of the system is $T = 298$ K, and the dielectric permittivity is $\varepsilon = 80\varepsilon_0$, where ε_0 is the vacuum permittivity. σ is the surface charge corresponding to nine deprotonated charge residues smeared over the filter walls:

$$\sigma = -\frac{9e}{2\pi R_f L_f}, \tag{A7}$$

where e is the proton charge and L_f is the length of the selectivity filter. For the sake of simplicity, we used a linear fit of the experimental NaCl activities from Robinson and Stokes (40):

$$\ln a_i = B \ln c_i + C, \tag{A8}$$

where $B = 0.9503$ and $C = -0.4053$. The error between the experimental and fitted activity is below 4.5% for concentration values up to 2 M. We took 0.2 nm for the hydrated radius of the Na^+ ions. This value is close to the Stokes radius (0.184 nm), and it is in between the crystallographic radius (0.095 nm) and the estimated hydrated radius in bulk solution (0.358 nm) (41). Therefore, we assume that the Na^+ ions hold the inner shell of water molecules when they cross the pore. The diffusion coefficients are used as fitting parameters (the starting values in the fitting process are the infinite dilution ones: $D_+^0 = 1.33 \times 10^{-9}$ m^2/s and $D_-^0 = 2.03 \times 10^{-9}$ m^2/s). The system of equations is solved numerically using the finite element method (42).

The PorA porin was kindly provided by Dr. Milan Blake. We thank Prof. Marco Colombini for fruitful discussions.

J.C. and V.M.A. gratefully acknowledge support from the Spanish Ministry of Education and Science (project FIS2004-03424).

REFERENCES

1. Nikaido, H. 2003. Molecular basis of bacterial outer membrane permeability revisited. *Microbiol. Mol. Biol. Rev.* 67:593–656.
2. Koebnik, R., K. P. Locher, and P. V. Gelder. 2000. Structure and function of bacterial outer membrane proteins: barrels in a nutshell. *Mol. Microbiol.* 37:239–253.
3. Karshikoff, A., V. Spassov, S. W. Cowan, R. Ladenstein, and T. Schirmer. 1994. Electrostatic properties of two porin channels from *Escherichia coli*. *J. Mol. Biol.* 240:372–384.
4. Cowan, S. W., T. Schirmer, G. Rummel, M. Steiert, R. Ghosh, R. A. Pauptit, J. N. Jansonius, and J. P. Rosenbusch. 1992. Crystal structures explain functional properties of two E. coli porins. *Nature*. 358:727–733.
5. Song, J. M., C. A. S. A. Minetti, M. S. Blake, and M. Colombini. 1999. Meningococcal PorA/C1, a channel that combines high conductance and high selectivity. *Biophys. J.* 76:804–813.
6. Brunen, M., H. Engelhardt, A. Schmid, and R. Benz. 1991. The major outer membrane protein of *Acidovorax delafieldii* is an anion-selective porin. *J. Bacteriol.* 173:4182–4187.
7. Mathes, A., and H. Engelhardt. 1998. Nonlinear and asymmetric open channel characteristics of an ion-selective porin in planar membranes. *Biophys. J.* 75:1255–1262.
8. Tommassen, J., P. Vermeij, M. Struyve, R. Benz, and J. T. Poolman. 1990. Isolation of *Neisseria-meningitidis* mutants deficient in class-1 (PorA) and class-3 (PorB) outer-membrane proteins. *Infect. Immun.* 58:1355–1359.
9. McGuinness, B., A. K. Barlow, I. N. Clarke, J. E. Farley, A. Anilionis, J. T. Poolman, and J. E. Heckels. 1990. Deduced amino-acid-sequences of class-1 protein (PorA) from 3 strains of *Neisseria meningitidis*—synthetic peptides define the epitopes responsible for serosubtype specificity. *J. Exp. Med.* 171:1871–1882.
10. van der Ley, P., J. E. Heckels, M. Virji, P. Hoogerhout, and J. T. Poolman. 1991. Topology of outer-membrane porins in pathogenic *Neisseria-Spp. Infect. Immun.* 59:2963–2971.
11. Jeanteur, D., J. H. Lakey, and F. Pattus. 1991. The bacterial porin superfamily—sequence alignment and structure prediction. *Mol. Microbiol.* 5:2153–2164.
12. Feavers, I. M., A. B. Heath, J. A. Bygraves, and M. C. J. Maiden. 1992. Role of horizontal genetic exchange in the antigenic variation of the

class-1 outer-membrane protein of *Neisseria-meningitidis*. *Mol. Microbiol.* 6:489–495.

13. Suker, J., I. M. Feavers, M. Achtman, G. Morelli, J. F. Wang, and M. C. J. Maiden. 1994. The PorA gene in serogroup A meningococci: evolutionary stability and mechanism of genetic variation. *Mol. Microbiol.* 12:253–265.
14. Derrick, J. P., R. Urwin, J. Suker, I. M. Feavers, and M. C. J. Maiden. 1999. Structural and evolutionary inference from molecular variation in *Neisseria* porins. *Infect. Immun.* 67:2406–2413.
15. Achouak, W., T. Heulin, and J.-M. Pages. 2001. Multiple facets of bacterial porins. *FEMS Microbiol. Lett.* 199:1–7.
16. Massari, P., S. Ram, H. Macleod, and L. M. Wetzler. 2003. The role of porins in neisserial pathogenesis and immunity. *Trends Microbiol.* 11:87–93.
17. Rosenqvist, E., E. A. Høiby, E. Wedege, K. Bryn, J. Kolberg, A. Klem, E. Ronnild, G. Bjune, and H. Nokleby. 1995. Human antibody responses to meningococcal outer membrane antigens after three doses of the Norwegian group B meningococcal vaccine. *Infect. Immun.* 63:4642–4652.
18. Milagres, L. G., M. C. A. Gorla, C. T. Sacchi, and M. M. Rodrigues. 1998. Specificity of bactericidal antibody response to serogroup B meningococcal strains in Brazilian children after immunization with an outer membrane vaccine. *Infect. Immun.* 66:4755–4761.
19. Phale, P. S., A. Philippsen, C. Widmer, V. P. Phale, J. P. Rosenbusch, and T. Schirmer. 2001. Role of charged residues at the OmpF porin channel constriction probed by mutagenesis and simulation. *Biochemistry.* 40:6319–6325.
20. Alcaraz, A., E. M. Nestorovich, M. Aguilella-Arzo, V. M. Aguilella, and S. M. Bezrukov. 2004. Salting out the ionic selectivity of a wide channel: the asymmetry of OmpF. *Biophys. J.* 87:943–957.
21. Aguilella-Arzo, M., J. J. Garcia-Celma, J. Cervera, A. Alcaraz, and V. M. Aguilella. 2007. Electrostatic properties and macroscopic electrodiffusion in OmpF porin and mutants. *Bioelectrochemistry.* 70:320–327.
22. Montal, M., and P. Mueller. 1972. Formation of bimolecular membranes from lipid monolayers and a study of their electrical properties. *Proc. Natl. Acad. Sci. USA.* 69:3561–3566.
23. Bezrukov, S. M., and I. Vodyanoy. 1993. Probing alamethicin channels with water-soluble polymers—effect on conductance of channel states. *Biophys. J.* 64:16–25.
24. Nestorovich, E. M., T. K. Rostovtseva, and S. M. Bezrukov. 2003. Residue ionization and ion transport through OmpF channels. *Biophys. J.* 85:3718–3729.
25. Jansen, C., A. Wiese, L. Reubsaet, N. Dekker, H. de Cock, U. Seydel, and J. Tommassen. 2000. Biochemical and biophysical characterization of in vitro folded outer membrane porin PorA of *Neisseria meningitidis*. *Biochim. Biophys. Acta.* 1464:284–298.
26. Colombini, M. 1989. Voltage gating in the mitochondrial channel, VDAC. *J. Membr. Biol.* 111:103–111.
27. Rostovtseva, T. K., T.-T. Liu, M. Colombini, V. A. Parsegian, and S. M. Bezrukov. 2000. Positive cooperativity without domains or subunits in a monomeric membrane channel. *Proc. Natl. Acad. Sci. USA.* 97:7819–7822.
28. Hille, B. 2001. Ion Channels of Excitable Membranes. Sinauer, Sunderland, MA.
29. Zambrowicz, E. B., and M. Colombini. 1993. Zero-current potentials in a large membrane channel: a simple theory accounts for complex behavior. *Biophys. J.* 65:1093–1100.
30. Levadny, V., and V. Aguilella. 2001. Reversal potential of a wide ion channel. Nonuniform charge distribution effects. *J. Phys. Chem. B.* 105:9902–9908.
31. Schuss, Z., B. Nadler, and R. S. Eisenberg. 2001. Derivation of Poisson and Nernst-Planck equations in a bath and channel from a molecular model. *Phys. Rev. E Stat. Nonlin. Soft Matter Phys.* 64:036116.
32. Kurnikova, M. G., R. D. Coalson, P. Graf, and A. Nitzan. 1999. A lattice relaxation algorithm for three-dimensional Poisson-Nernst-Planck theory with application to ion transport through the Gramicidin A channel. *Biophys. J.* 76:642–656.
33. Cardenas, A. E., R. D. Coalson, and M. G. Kurnikova. 2000. Three-dimensional Poisson-Nernst-Planck theory studies: influence of membrane electrostatics on Gramicidin A channel conductance. *Biophys. J.* 79:80–93.
34. Hollerbach, U., D. P. Chen, D. D. Busath, and B. Eisenberg. 2000. Predicting function from structure using the Poisson-Nernst-Planck equations: sodium current in the Gramicidin A channel. *Langmuir.* 16:5509–5514.
35. Im, W., and B. Roux. 2002. Ion permeation and selectivity of OmpF porin: a theoretical study based on molecular dynamics, Brownian dynamics, and continuum electrodiffusion theory. *J. Mol. Biol.* 322: 851–869.
36. Koumanov, A., U. Zachariae, H. Engelhardt, and A. Karshikoff. 2003. Improved 3D continuum calculations of ion flux through membrane channels. *Eur. Biophys. J.* 32:689–702.
37. Goldman, D. 1943. Potential, impedance and rectification in membranes. *J. Gen. Physiol.* 27:37–60.
38. Hodgkin, A., and B. Katz. 1949. The effect of sodium ions on the electrical activity of the giant axon of the squid. *J. Physiol.* 108:37–77.
39. Sims, S. M., W. I. Higuchi, V. Srinivasan, and K. Peck. 1993. Ionic partition-coefficients and electroosmotic flow in cylindrical pores: comparison of the predictions of the Poisson-Boltzmann equation with experiment. *J. Colloid Interface Sci.* 155:210–220.
40. Robinson, R. A., and R. H. Stokes. 1959. Electrolyte Solutions. Butterworths, London.
41. Conway, B. E. 1981. Ionic Hydration in Chemistry and Biophysics. Elsevier Scientific Publishing, Amsterdam.
42. Lucquin, B., and O. Pironneau. 1998. Introduction to Scientific Computing. Wiley, New York.